Mechanical Studies of Single Ribosome/mRNA Complexes

Francesco Vanzi,* Yasuharu Takagi,† Henry Shuman,* Barry S. Cooperman,‡ and Yale E. Goldman*
*Pennsylvania Muscle Institute, †Department of Bioengineering, and ‡Department of Chemistry, University of Pennsylvania, Philadelphia, Pennsylvania

ABSTRACT Methodology was developed for specifically anchoring *Escherichia coli* 70S ribosomes onto a chemically modified, cysteine-reactive glass surface. Immobilized ribosomes maintain the capability of binding a polyuridylic acid (poly(U)) template, enabling investigation of mechanical properties of individual ribosome-poly(U) complexes using laser tweezers. Streptavidin-coated polystyrene microspheres bound specifically to the biotinylated 3′ end of long (up to 10,000 bases) poly(U) strands. A novel optical method was built to control the position of the laser trap along the microscope optical axis at 2 nm resolution, facilitating measurement of the force-extension relationship for poly(U). Some immobilized ribosome-poly(U) complexes supported 100 pN of force applied at the 3′ end of the mRNA. Binding of *N*-acetylated Phe-tRNA^{Phe}, an analog of the initiator fMet-tRNA^{Met}, enhanced the population of complexes that could withstand high forces. The persistence length of poly(U) RNA homopolymer, modeled as a worm-like chain, was found to be 0.79 ± 0.05 nm and the backbone elasticity was 900 ± 140 pN, similar to values for single-stranded DNA.

INTRODUCTION

Ribosomes are responsible, in all living cells, for the synthesis of proteins coded by template mRNAs. The initiation, elongation, and termination of peptide synthesis are accomplished by the ribosomes in conjunction with accessory proteins, soluble tRNAs, and metabolic energy. During elongation of the nascent peptide, the process of selection of the correct aminoacyl-tRNA and formation of a peptide bond between the growing peptide and the incoming amino acid occurs on the ribosome with high speed (~20 peptide bonds/s (1,2)) and accuracy (error frequency on the order of 10^{-4}, (3)). Although remarkable progress has been made recently on the structural biology and biochemistry of the ribosome and the peptide elongation cycle (4–11), the dynamics and structural mechanisms of several steps are not fully understood, such as proofreading of the amino acid selection and maintenance of the codon reading frame.

The development and application of single-molecule techniques has advanced our understanding of the physical properties and functional mechanisms of enzymes and nucleic acids. Some of the mechanisms involved in protein synthesis may potentially be elucidated by exploitation of these techniques with individual ribosomes and mRNAs. The elastic properties of nucleic acids have been deduced from bulk measurements (12–14) and various single-molecule techniques (15–21). These measurements provide understanding of the physical properties of nucleic acids which impact on their biological function. For example, the flexibility of DNA is an essential parameter in the energetics of its condensation into chromatin and packaging into viral capsids (22). The mechanical properties of a nucleic acid polymer molecule can be resolved into components arising from the elasticity of the polymer backbone, sequence-dependent base stacking, and secondary and tertiary structures. Most experimental attention has been given to single- and double-stranded DNA, but some force-extension (F-E) measurements on small RNA molecules have also been presented (23), with particular attention to the folding and unfolding of secondary structures. Measurement of the elastic properties of mRNA is an essential step for development of single-molecule mechanical assays of ribosomal function because knowledge of the template F-E curve is required to interpret force-velocity curves in nucleic acid processing enzymes (24) and to understand how mRNA secondary structure modulates overall translation rates (25,26) as well as pauses in translation and programmed frame shifts during protein synthesis (27).

Blanchard et al. (28,29) have recently reported single-molecule fluorescence energy transfer experiments on functioning ribosomes that give insights into tRNA dynamics and proofreading. The ribosomes were localized near the microscope slide surfaces via their binding to immobilized mRNA. For mechanical measurements in which force is applied, however, it is necessary to employ an attachment directly on the ribosome. We have previously reported methods for nonspecific immobilization of ribosomes on the surface of mica coverslips (30) and for detection of their peptide synthetic activity (31). However, birefringence renders mica unsuitable for many high resolution optical methods. Here, we describe an improved method of immobilization, allowing selective recruitment of ribosomes onto a chemically modified glass surface while retaining their ability to bind polyuridylic acid (poly(U)) mRNA. Such binding allows

Submitted November 13, 2004, and accepted for publication May 23, 2005.

Address reprint requests to Yale E. Goldman, Pennsylvania Muscle Institute, School of Medicine, University of Pennsylvania, Philadelphia, PA 19104-6083. Tel.: 215-898-4017; Fax: 215-898-2653; E-mail: goldmany@mail.med.upenn.edu.

Francesco Vanzi's present address is Dipartimento di Biologia Animale e genetica, via Romana 17, 50100 Florence, Italy.

0006-3495/05/09/1909/11 $2.00

doi: 10.1529/biophysj.104.056283

measurement, using optical microscopy and infrared laser tweezers, of the strength of the ribosome-poly(U) complex, the influence of ambient solution conditions on this strength, and the elastic properties of the poly(U). This single-stranded homopolymer is devoid of secondary structure and thus allows direct measurement of the backbone F-E curve (32,33). We also measured the effect of adding an initiator-tRNA analog (*N*-acetylated Phe-tRNA^{Phe}) on the mechanical strength of the ribosome-poly(U) complex, demonstrating that surface-bound ribosomes bind *N*-acetylated Phe-tRNA^{Phe}, which strengthens the mRNA-ribosome bond. Preliminary reports have appeared in abstract form (32,34).

MATERIALS AND METHODS

The laser trap apparatus

The setup (Fig. 1), built around an inverted microscope (Nikon (Tokyo, Japan) Diaphot 300) and mounted on an antivibration optical table (I-2000 Stabilizer; Newport, Irvine, CA), has been briefly described by Litvinov et al. (35). The output beam of a 1064 nm Nd:YAG laser (Spectra Physics (Mountain View, CA) model T20-B-106C-01) is expanded and split into two beams with a polarizing beam splitting prism (PBS1 in Fig. 1), producing two independent traps at the sample plane. The stage position of one of these traps is mechanically adjustable using mirrors M1 and M2. The other one is electronically deflected in both *x* and *y* directions at the sample by two acousto-optic deflectors (AODs). The two polarized beams are recombined by PBS2, shaped further, and reflected into the optical axis of the microscope using a dichroic mirror (DM1). The overall beam expansion is sufficient to fill the back focal plane aperture of the microscope objective (Nikon Fluor 100× oil immersion, 1.3 numerical aperture). The sample is mounted on a piezo-stage capable of three-dimensional control of position with nanometer resolution (Queensgate Instruments (Torquay, UK) NPS-3330).

The distribution of infrared (IR) light at the back focal plane of the condenser is an indication of the laser trap force on the bead, relatively independent of the trap position (36,37). The back focal plane intensity distribution for each of the traps is separated according to its polarization by PBS3 and imaged onto separate quadrant photodiodes for recording of the trap-bead forces (35). *x*- and *y*-directed force signals for the H-polarization and V-polarization photodiodes corresponding to the two traps were in each case detected from lateral deflection of the transmitted IR light by combining the photodiode currents of the quadrant photodiodes, $I_A + I_B - I_C - I_D$ and $I_A + I_C - I_B - I_D$ (Fig. 1). The calibration of the force signals is described in the online Supplementary Material.

Mechanical drift of the trap positions along the *z* axis in significant amounts relative to the length of our sample RNA polymers led us to develop a method to measure and control the *z*-position. This system uses IR light reflected from the back of the experimental microscope coverslip (*dashed orange lines* in Fig. 1), an astigmatic optical system similar to the focus-tracking control of a compact audio disc player (38), and additional detectors (*Camera 2* and *z* axis quadrant photodiode in Fig. 1). The ellipticity of the reflected light distribution at the *z*-position quadrant photodiode, detected from the combination of photocurrents $I_A + I_D - I_B - I_C$, is a sensitive measure of the trap height above the microscope coverslip. This signal is fed back through the experimental driving software to reposition the *z* axis of the piezo-electric stage, nulling the drift after each experimental trace (every 8 s); ~5–7% of the total laser power is used in the *z*-detection beam.

The *z* axis system is calibrated by monitoring the effect on the visco-elastic cutoff frequency of a trapped bead as it is brought very near to the coverslip surface (see Supplementary Material and Happel and Brenner (39) and Svoboda and Block. (40)). The resolution of this method as used during experimental recording, with photodiode signals sampled at 2 kHz and averaged over for 50 ms, was ~2 nm. Details of this enhancement to the optical trap and its validation will be published elsewhere.

Preparation of cysteine-reactive coverslips

Glass microscope coverslips were functionalized with amine groups using 3-aminopropyltriethoxysilane (APTES, United Chemical Technologies,

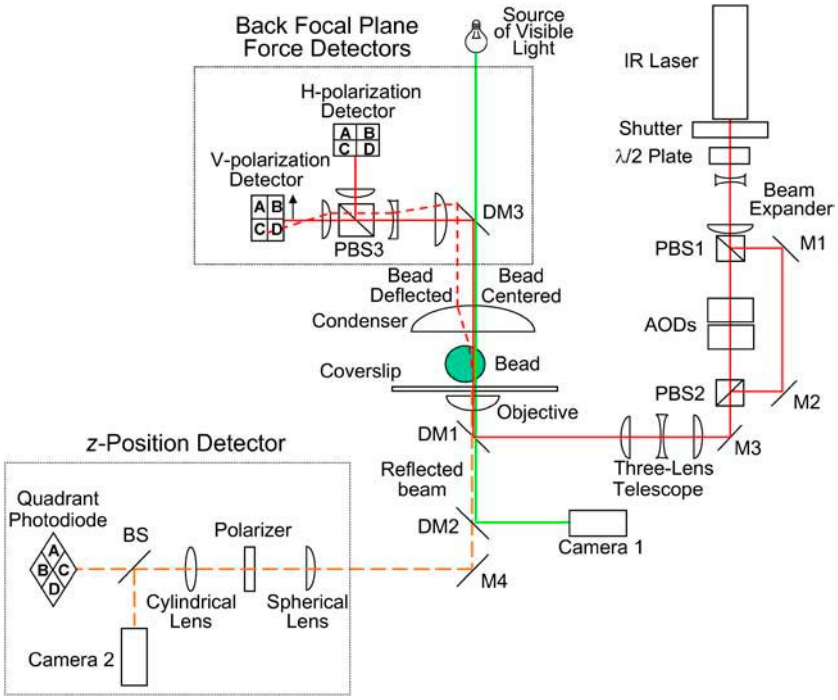

FIGURE 1 Schematic diagram of the laser tweezers apparatus. Abbreviations: M (mirror); PBS (polarizing beam splitter); BS (beam splitter, unpolarized); and DM (dichroic mirror). The red line represents the path of the IR optical trap laser beam. Above the sample, the solid red line represents the path of the beam in the absence of a bead or with a bead centered in the beam. The dashed red line represents the path of the IR beam deflected by an off-axis bead. The dashed orange line represents the IR light reflected at the glass-water interface of the sample chamber. The green line represents visible light, used to illuminate the sample and image it on Camera 1.

Bristol, PA; reagent 919-30-2) followed by treatment with *N*-[k-Maleimidoundecanoyloxy]sulfosuccinimide ester (Sulfo-KMUS) (21111) (Pierce, Rockford, IL) a heterobifunctional cross-linker carrying a succinimide group at one end, an 11-carbon linker chain, and a maleimide group at the other end. The succinimide group reacts with the amines on the surface, attaching the KMUS to the slide and leaving its maleimide groups exposed and reactive toward protein sulfhydryls at the surface of the ribosome.

Glass coverslips were washed with RNAase Away (Molecular Bio-Products, San Diego, CA) and rinsed with RNAase-free water. They were then submerged in ethanol, sonicated at room temperature for 5 min, dried at 110°C for 30 min, and then exposed to a reactive ion plasma in a radio-frequency plasma cleaner (Harrick (Pleasantville, NY) PDC-32G) for 5 min. To derivatize the glass surface with amines, the clean coverslips were treated for 5 min at room temperature with a solution of 2% (v/v) APTES in acetone. This treatment was followed by washing with acetone and deionized water and drying overnight at room temperature to allow condensation of the silane.

The coverslips were next incubated for 2 h at room temperature with a solution containing 0.5 mM Sulfo-KMUS in 20% (v/v) HEPES 100 mM (pH 7.5) and 80% (v/v) dimethyl sulfoxide (DMSO), followed by five washes with deionized water and a 2-h incubation at room temperature in 50 mM acetic acid *N*-hydroxysuccinimide ester (ICN 100020). The latter reagent was used to acetylate any surface amines that had not reacted with the KMUS. The coverslips were again washed five times with deionized water and dried overnight at room temperature. The prepared coverslips were stored at room temperature in a clean hood and used over a period of several weeks without observable changes in their reactivity.

Biochemical reagents

High-molecular weight poly(U) (average length 8,000–10,000 bases) was prepared by polynucleotide phosphorylase polymerization of UDP, fractionated by Sephacryl column chromatography, and selectively biotinylated at the 3′ end as described earlier (31). *Escherichia coli* Q13 70S ribosomes were prepared as described (41). *N*-acetyl-PhetRNA^{Phe}, prepared as in Rappoport and Lapidot (42), was a gift of Dr. M. Ehrenberg, Uppsala University, Sweden.

Formation of poly(U)-ribosome complexes on the KMUS surface

A flow chamber was constructed by joining a KMUS-treated coverslip and a standard 1 mm thick microscope slide using double-sided adhesive tape to form a 12–17 μl flow chamber. All reagents and washes, except where noted, were made in TMK buffer (50 mM Tris/HCl, pH 7.5; 10 mM $MgCl_2$; 50 mM KCl). 70S ribosomes were applied at a concentration of 1.2 nM and incubated for 2 h at room temperature in a moist environment to avoid evaporation. Unreacted ribosomes were removed by five washes with TMK buffer. Then, 0.2 mM L-cysteine (Sigma (St. Louis, MO) C-9768) was applied and incubated for 30 min to block any maleimide groups that had not reacted with ribosomes. After five more washes, 5 mg/ml acetylated bovine serum albumin (B-2518, Sigma) was flowed into the chamber and incubated for 20 min to saturate surface sites with nonspecific affinity for proteins. This was followed by a 20 min incubation with a solution of long biotinylated poly(U) at ~100 nM concentration. After five more washes, a 0.05% (w/v) suspension of streptavidin-coated 1.2 μm diameter polystyrene microspheres (Bangs Laboratories (Fishers, IN)CP01F-5134, prewashed twice with TMK buffer before use), in TMK supplemented with 5 mg/ml acetylated bovine serum albumin, was applied and allowed to incubate for 2 h. After 10 TMK washes to remove unbound beads, the slide was sealed with clear nail polish, unless the experiment required further solution exchanges during observation at the microscope.

Measurement of F-E curves

When a sample for microscopic observation was prepared with ribosomes, long biotinylated poly(U) template, and streptavidin-coated microspheres as described above, three populations of beads could usually be distinguished: beads freely diffusing in solution, beads undergoing restricted diffusion, and beads immobilized on the surface. The parameter used to quantify the range of diffusion is the root mean-squared deviation (D_{rms}) of the bead centroid over a time of 30–120 s. Tethered beads have a much larger D_{rms} than immobilized beads, but they remain within the field of observation. Free beads, on the other hand, display the expected continuous increase in D_{rms} with (square root of) time and diffuse out of the field of observation in just a few seconds. In the experiments described here, beads were classified as ''tethered'' when they displayed a D_{rms} larger than 100 nm.

A tethered bead was brought close to the position of the optical trap by moving the stage in the *x*, *y* plane with micromanipulators. The trap was briefly switched on to verify that the center of the bead's restricted diffusion was within a few hundred nm of the trapped position. The height of the trap was set to 800–900 nm, providing 200–300 nm clearance between the coverslip surface and the bottom of the trapped bead. A LabView script (National Instruments (Austin, TX) V5.1) controlled the stage and data acquisition by performing the following steps to record the F-E curve of the poly(U), stretching the molecule in the *x* direction and then in the *y* direction: 1), the initial position of the trap on the *z* axis was measured; 2), a triangular wave of preset amplitude and frequency was applied to the stage position in the *x* direction; 3), when the stage returned to its original position on the *x* axis, the height of the trap (*z*-position) was measured again and reset to its initial value to cancel drift; 4), steps 2 and 3 were repeated 2–3 times; and 5), steps 2–4 were repeated as the stage moved in the *y* direction.

The triangular-wave motion of the stage was generated as a succession of small steps (20 nm to 140 nm in different recordings) applied at 100 ms intervals. The output voltages of the *x*- and *y*-force detectors and of the *z*-position detector were sampled at 2 kHz for 50 ms at each step position. Serial communication between the computer and the stage controller for recording its position (x_{st} and y_{st}) and executing the next step took the remaining 50 ms.

If at the end of one set of *x* and *y* F-E recordings the bead was still tethered, measurements were repeated with an increased step size until the tether was broken, as shown by the force abruptly declining to zero and the bead freely diffusing in the medium once the trap was turned off. The data were analyzed and corrected for various instrumental and mechanical factors essentially as described by Wang et al. (16), extending the geometric force and distance calculation to all three dimensions as described in the online Supplementary Material.

Two main theoretical models were tested for extracting parameters describing the elastic properties of the poly(U): the freely jointed chain (FJC) and the worm-like chain (WLC). Each model was supplemented with a parameter allowing for compliant extension of the backbone, (16). These models lead to F-E relations:

$$L = L_c\left[\coth\left(\frac{Fb}{k_BT}\right) - \frac{k_BT}{Fb}\right] \text{ ''FJC''} \quad (1)$$

$$F = \frac{k_BT}{L_p}\left[\frac{1}{4(1-L/L_c)^2} - \frac{1}{4} + \frac{L}{L_c}\right] \text{ ''WLC''} \quad (2)$$

$$L = L_c\left[\coth\left(\frac{Fb}{k_BT}\right) - \frac{k_BT}{Fb}\right]\left(1+\frac{F}{K}\right) \text{ ''Extensible FJC''}. \quad (3)$$

$$F = \frac{k_BT}{L_p}\left[\frac{1}{4(1-L/L_c+F/K)^2} - \frac{1}{4} + \frac{L}{L_c} - \frac{F}{K}\right] \text{ ''Extensible WLC''} \quad (4)$$

In these equations, L is the end-to-end length of the polymer, L_c is the contour length, F is the force, L_p is the persistence length (a measure of the bending stiffness), b is the Kuhn length (equivalent to $2\,L_p$ at low force), K is the stretch modulus (the force that would be necessary to extend the polymer backbone to twice its contour length), k_B is Boltzmann's constant, and T is the temperature. These equations were fitted to the corrected F-E data by minimizing the squared force residuals using the solver in MathCad (Mathsoft, Cambridge, MA) V2001Pro).

Each F-E curve was measured repeatedly, typically 4–6 times. A standard deviation, σ_i, of the mean force data at each extension was calculated, and the χ_r^2 value was calculated as

$$\chi_r^2 = \frac{1}{\nu}\sum_i \left[\frac{F_i - F(L_i)}{\sigma_i}\right]^2,$$

where ν is the number of experimental data points minus the number of fitted parameters, F_i is the measured value of force of the i^{th} sample (measured at extension L_i), and $F(L_i)$ is the force value predicted by the particular model under test at extension L_i . The χ_r^2 values for the four models were used as figures of merit to compare their quality of fit. Confidence (95%) intervals for the fitted parameters were estimated by probing the χ_r^2 surface and finding the extreme values of each parameter at a $\chi_r^2 < 4$ (43).

Strength of poly(U)-ribosome complexes on KMUS

The samples were prepared as described above except in some experiments, *N*-acetyl-PhetRNA^{Phe} (42) was added. The procedure used to select beads and acquire data was very similar to that used in the F-E measurements, with the exception that only one large ramp was applied to the stage to progressively stretch the polymer molecule up to a force that would rupture the tethered complex. This ramp comprised 100 steps, 40 nm in amplitude and applied at 100 ms intervals. A lower trap stiffness (κ_x ~0.07 pN/nm; κ_y ~0.04 pN/nm) was used to improve the accuracy of force measurement in the 1–25 pN range.

RESULTS

Binding of ribosomes to the KMUS surface

Microscope coverslips, made cysteine reactive by treatment with APTES and Sulpho-KMUS, a succinimide-maleimide cross-linking reagent, were used to assemble flow chambers and treated successively with 70S ribosomes, very long poly(U) RNA biotinylated at the 3′ end, and finally, streptavidin-coated polystyrene beads as explained in Materials and Methods. Among the beads bound to the surface, two populations were distinguished: beads that were completely immobilized, surface density (hereinafter denoted density) averaging $1.7 \pm 0.4 \times 10^{-3}$ beads per μm^2, and beads that displayed Brownian diffusion within a 150–250 nm restricted range, average density $2.4 \pm 0.4 \times 10^{-3}$ beads/μm^2. The latter class of beads was considered to represent complexes in which the bead tags the 3′ end of a long poly(U) molecule tethered to the surface by a ribosome.

When both 70S ribosomes and poly(U) were omitted, markedly fewer beads bound to the surface (Fig. 2). The density of tethered and immobilized beads was reduced 70-fold and 6-fold, respectively. Omission of either 70S ribosomes or poly(U) reduced the density of both immobilized and tethered beads almost to background levels (Fig. 2, 70S and poly(U) bars).

These observations strongly support the view that almost all of the tethered beads represent complete linkages, i.e., beads bound to the 3′ end of a poly(U)-ribosome complex. The significant density above background of immobilized beads in the sample prepared fully with 70S ribosomes and poly(U) suggests that some of the complete linkages do not undergo measurable restricted diffusion, most likely because the tether is too short.

When the KMUS surface was pretreated with β-mercaptoethanol (β-ME, 150 mM, 1 h at room temperature) before adding the ribosomes and other components, the densities of tethered beads and immobilized beads were reduced ~9-fold and 2-fold, respectively. Similarly low densities of beads were obtained if either KMUS or APTES were omitted. These results indicate that most of the ribosomes carrying complete complexes are bound specifically to the surface through the APTES and KMUS.

F-E curves of poly(U) bound to ribosomes

To collect poly(U) F-E data from beads tethered to the surface, the stage was moved alternatively in the x and in the y direction (Fig. 3 *A*). The force response (Fig. 3 *B*) is evident mainly in the direction of motion, whereas the orthogonal component of force is small. On a faster time scale (Supplementary Material Fig. S3), the force signal was essentially constant between steps, indicating, as expected, that the mechanical behavior of the poly(U) was close to purely elastic, with a negligible viscous component. In this experiment, the height of the trap (Fig. 3 *C*) was maintained at

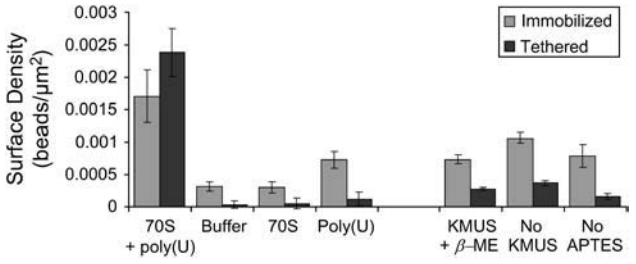

FIGURE 2 Surface density of microspheres on KMUS. For each condition, the light shaded bar describes the density of immobilized beads and the dark bar describes the density of tethered beads observed on the microscope slide. The set of bars on the left side describes the dependence of the density on the presence of 70S ribosomes (70S) and/or poly(U). The bar labeled ''Buffer'' refers to a sample in which buffer was used in place of both ribosomes and poly(U). The bars on the right side show the density in the presence of both 70S ribosomes and poly(U) on a KMUS surface pretreated with β-ME, on a surface prepared omitting the KMUS treatment, and on a surface prepared omitting the APTES. Values plotted are mean ± SE. From left to right the values for the number of microscopic fields observed (in two slides for 70S + poly(U) and one slide each for all the other conditions) are 34, 32, 23, 20, 10, 5, and 7.

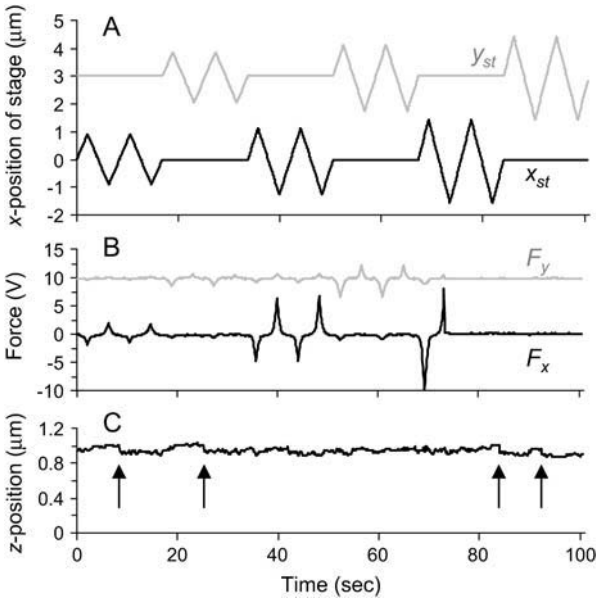

FIGURE 3 Recording of F-E data. (*A*) Measured position of the stage in the *x* direction (*black trace*) and in the *y* direction (*shaded trace*, offset for clarity). (*B*) Recorded output of the force detector (in volts) for the *x* direction (*black trace*) and the *y* direction (*shaded trace*, offset for clarity). Rupture of the complex occurs at ~75 s while the stage is moving in the *x* direction. (*C*) Measured height of the trap; the arrows indicate points at which feedback restoration of the height to its initial value is apparent.

950 nm above the coverslip surface by the feedback system described in Materials and Methods. Some of the height adjustments to correct *z* axis drift are marked by arrows in Fig. 3 *C*. Most F-E recordings were terminated by an abrupt decrease of force to zero while the stage was still moving (Fig. 3 *B* at ~75 s), presumably indicating rupture of the poly(U)-ribosome complex. After such an event, force remained zero during further movements of the stage and, when the trap was turned off, the bead diffused away freely.

As described in the Supplementary Material, estimation of the polymer length required calculating the deflection of the bead from the center of the trap using the ratio of measured force and displacement in the *x*, *y* plane and the trap stiffness in the *z* direction. The trap height, z_t, was measured continuously (Fig. 4, *triangles*). The estimate of bead height (z_b, *circles* in Fig. 4) deviates from this value mainly at large excursions of the stage position, x_{st}, due to the *z* component of the stretching force. However, an artifactual deviation between z_t and z_b is also evident near zero excursion due to very low values of both force and displacement. Fitting of a sixth order polynomial to all z_b values except for the few central ones and interpolating near zero (*line* in Fig. 4) show that z_b approaches z_t at the ribosome position, x_0 (*vertical dashed line*). Essentially the same F-E curves were obtained either substituting the interpolated points near x_0 for the artifactual central measurements or ignoring the central measurements altogether.

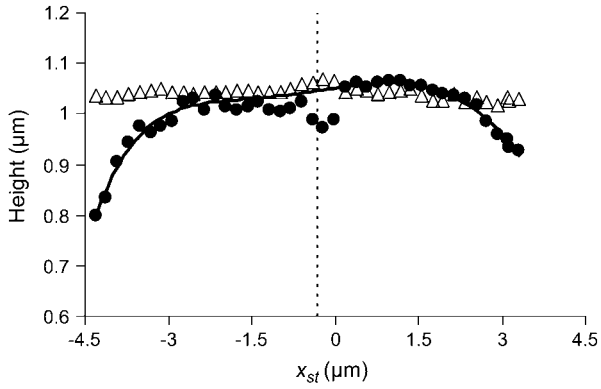

FIGURE 4 Height of the trap and of the center of the microsphere. The triangles show the measured values of the trap height (z_t) during one cycle of F-E measurements with the stage moving in the *x* direction. The solid circles show the height of the center of the bead (z_b) calculated as described in the Supplementary Material. x_{st} is the stage position. The dotted vertical line shows the position of x_0 (see text for details). The solid curve represents a sixth order polynomial fit to the z_b data, excluding the three points nearest x_0. As expected, this curve approaches z_t for $x_{st} = x_0$.

Fig. 5 shows the magnitude of the different corrections introduced in calculating the F-E curve for a typical bead-poly(U)-ribosome complex. The solid symbols represent F-E data measured moving the stage along the *x* axis. The dark blue symbols are the raw data of force versus position of the center of the trap. Correction for the deflection of the *x*-position of the bead from the center of the trap (described in the Supplementary Material) causes a reduction of the extension, with no change to the measured force (*red squares*). Further correction for the *y* and *z* components of deflection leads to the F-E curve of the complex along the applied axis of force but which still incorporates the radius of the bead in the plotted extension (*cyan symbols*). Differences

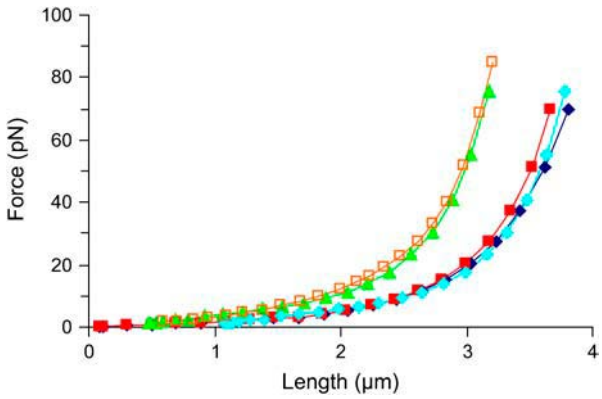

FIGURE 5 Magnitude of corrections in the calculation of the F-E curve. The dark blue symbols are the raw data of force versus position of the center of the trap stepping the stage along the *x* axis. The corrections applied are as follows: deflection of the *x*-position of the bead from the center of the trap (*red squares*); correction for the *y* and *z* components (*cyan symbols*); subtraction of the bead radius (*green symbols*). The orange squares show the corresponding corrected F-E curve measured in the *y* direction.

between the raw and corrected data (*blue* versus *cyan symbols*) are small up to forces of ~20 pN due to the relatively high trap stiffness. Subtracting the bead radius (600 nm) from the overall distance values (*cyan symbols*) gives the F-E curve of the poly(U) itself (*green symbols*). The corresponding corrected F-E curve for the same poly(U) molecule, measured in the *y* direction, is very similar (*orange squares*).

Parameters describing the elastic behavior of the poly(U) were determined by fitting four models of extensible polymers to the data (Fig. 6) as described in Materials and Methods. The FJC and WLC models without provision for extension of the polymer backbone (Eqs. 1 and 2 in Materials and Methods, *magenta* and *red curves* in Fig. 6) do not describe the data well, in agreement with previous data reported for DNA (16). The deviations are especially marked at low forces. Also, these two models predict higher slopes at high extensions than exhibited by the data, suggesting that introducing a stretch modulus for the backbone would improve the fit. Adding backbone extensibility to the models (Eqs. 3 and 4 in Materials and Methods) improved the fits markedly (*green* and *brown curves* in Fig. 6).

The parameters and statistics obtained by fitting the four different models to 32 molecules are given in Table 1. Introduction of the extra fitting parameter (K) allowing for backbone extension lowers the value of χ^2_r by a factor of 5 for the FJC model (extended FJC (E-FJC) versus FJC) and ~3 for the WLC model (extended WLC (E-WLC) versus WLC). Differences between the parameters obtained from E-FJC and E-WLC models were small, but the E-WLC model yielded the lowest values of χ^2_r and was therefore chosen for the remaining analysis.

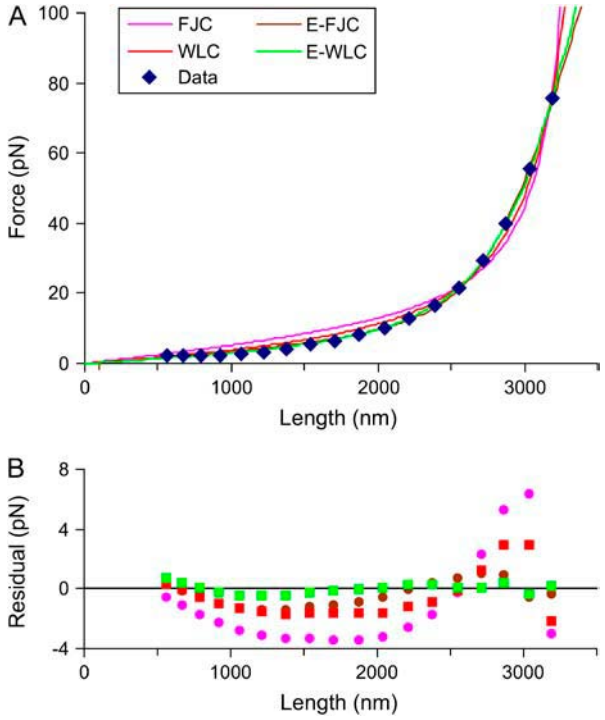

FIGURE 6 Comparison of four models fitted to the F-E curve of a poly(U) molecule. (*A*) F-E curve measured for one poly(U) molecule and theoretical fits. Blue diamonds: experimental data. The fitted curves represent the FJC (*magenta*), E-FJC (*brown*), WLC (*red*), and E-WLC (*green*). (*B*) Residuals between fit and experimental data with the same color code.

Using the E-WLC model, the measured value for persistence length, L_p, for poly(U) was 0.79 ± 0.05 nm (mean ± SE, $n = 32$), in excellent agreement with the value of 0.75 nm reported for single-stranded DNA (ssDNA; Smith et al. (18) reported Kuhn length, 1.5 nm corresponding to $L_p = 0.75$ nm; (20)). The estimated stretch modulus (K) was 870 ± 140 pN (mean ± SE, $n = 24$), in good agreement with the values of 800–1000 pN reported for ssDNA (18). The values of L_c measured for each molecule varied from ~1000 nm to ~4000 nm. This wide distribution was expected from the range of lengths present in the poly(U) preparation used and because ribosomes can probably bind to a poly(U) molecule at any position along its length. The average value of L_c was 1910 ± 130 nm ($n = 32$) for poly(U) molecules averaging 6,500 bases, estimated by agarose gel chromatography (31).

The influence of the length of the polymer on the F-E measurements was tested with a sample of poly(U) containing shorter molecules, ~3000 bases according to their mobility on agarose gels (31). The values of mechanical parameters obtained with this preparation of poly(U) were $L_p = 0.80 \pm 0.09$ nm ($n = 4$ beads), $K = 845 \pm 270$ pN, very similar to the values given above with longer poly(U), whereas the measured $L_c = 990 \pm 190$ nm was ~½ the value from the longer RNA. These results were expected since L_p and K are intrinsic properties of the poly(U), whereas L_c is proportional to the number of bases in each particular molecule.

An estimate of the increment, d, to L_c per base along the backbone can be made by dividing the measured values of L_c by half of the average base length of the poly(U), on the

TABLE 1 Results of fitting quantitative models to poly(U) F-E data

	L_p (nm)	L_c (nm)	K (pN)	χ^2_r
FJC	0.46 ± 0.03	1870 ± 120	n.a.	11 ± 2
E-FJC	0.65 ± 0.03	1670 ± 120	570 ± 60 (30)	2.3 ± 0.6
WLC	0.57 ± 0.03	2130 ± 140	n.a.	3.6 ± 0.7
E-WLC	0.79 ± 0.05	1910 ± 130	870 ± 140 (24)	1.1 ± 0.2

Equations for each of these models are given in Materials and Methods. The persistence lengths (L_p) derived from the FJC models are obtained by dividing b (the Kuhn length) by 2. The numbers indicated are means and standard errors of the mean. Where not indicated, $n = 32$. For the determination of K, only the fits that showed a lower χ^2_r for the extensible model than the inextensible version of the same model were used, and the number of samples used is indicated in parentheses. The number of samples used to obtain the mean ± SE of K is lower than 32 because some F-E traces did not reach forces high enough to properly constrain the value of K when fitting the E-WLC model, leading to very large uncertainty on the fitted value of K.

assumption that ribosome binding is equally likely anywhere along the poly(U), so that the average position is midway along its length. This procedure gives estimates for d of 0.66 nm and 0.59 nm for the shorter and longer poly(U)s, respectively. These values are quite similar to each other and to the contour length increment per base estimated for ssDNA (0.6–0.7 nm (18,44)).

Based on the value for d of 0.66 nm per base, the dispersion of the values measured for L_p (standard deviation 720 nm, corresponding to ~1,200 bases) is quantitatively in agreement with the observed range of lengths in the poly(U) preparations used for these measurements.

Strength of poly(U)-ribosome complexes

Fig. 7 shows examples of recordings obtained when the stage was moved to progressively pull tethered beads away from the center of their restricted diffusion and the linkage between the bead and the coverslip ruptured. The intensity of the trap laser was reduced for measurements of the breaking force to improve resolution in the measurement of forces below 20 pN. In this condition, the force sufficient to pull a bead out of the trap is 22–25 pN, this value representing the upper limit of forces measurable at the low trap intensity. The most common result was that the force increased monotonically until the complex broke and force abruptly decayed to zero (Fig. 7 *A*). Some traces (~25%) displayed single or multiple ''slippage'' events in which the force abruptly decreased but subsequently developed again upon further displacement of the stage (Fig. 7 *B*), indicating that the bead was still tethered to the surface.

The complexes divided into two groups, those rupturing during a recording (90%) and those not rupturing even on application of a 25 pN force (10%). Fig. 8 *A* shows the distribution of rupture forces measured on 218 complexes. The complexes that ruptured at force <25 pN partitioned into three apparent groups, with rupture forces $F < 6$ pN, 6 pN $< F <$ 15 pN, and 15 pN $< F <$ 25 pN. The sum of three Gaussian components was fitted to the distribution using the maximum likelihood method (43). From the χ^2_r values obtained with fewer components, the data warranted fitting with all three components. The fraction of each component is indicated in Fig. 8 *A*.

Addition of *N*-AcPhe-tRNA^{Phe} is expected to strengthen ribosome-poly(U) interaction via basepairing with poly(U) in the ribosomal P-site. Interestingly, such addition, although leaving unaltered both the shape of the distribution of rupture forces (Fig. 8 *B*), which retains three components below 25 pN, and the positions and widths of the peaks, did change the relative populations of the peaks. Addition of *N*-AcPhe-tRNA^{Phe} decreased the proportion of complexes rupturing at the lower forces and increased the proportion rupturing at higher forces. For instance, 101 out of 218 complexes ruptured at forces <15 pN in the absence of *N*-AcPhe-tRNA^{Phe}, whereas only 69 complexes out of 214 broke at <15 pN in the presence of *N*-AcPhe-tRNA^{Phe}. Using the 'test of independence' among these classes (45), the level of significance of this difference is $p < 0.01$. Thus, our results are in accord with the expected strengthening of the ribosome-poly(U) interaction on addition of *N*-AcPhe-tRNA^{Phe}.

Added *N*-AcPhe-tRNA^{Phe} also doubles the proportion of complexes exhibiting apparent slippage before complete rupture (Fig. 7 *B*) from 43 out of 215 to 84 out of 213. The difference in these proportions is dependent on added *N*-AcPhe-tRNA^{Phe} at $p < 0.005$ significance.

DISCUSSION

Functional immobilization of ribosomes on surfaces

To apply single-molecule mechanical analysis toward the understanding of protein synthesis, methods are required that immobilize ribosomes onto a surface while maintaining their enzymatic activity. We report a method for specific attachment of ribosomes through their surface-exposed cysteines, using a bifunctional cross-linker to form a strong covalent connection to a chemically functionalized glass surface. Ribosomes recruited to the surface by this route bound long molecules of poly(U) mRNA, enabling study of the mechanics of the mRNA-ribosome complex.

Previous studies of ribosomes immobilized on surfaces included immobilization of mRNA to surfaces and subsequent recruitment of ribosomes (28,29,46) and nonspecific adsorption of 70S ribosomes to mica (30). In the latter case, puromycin activity at the peptidyl transferase site (30) and

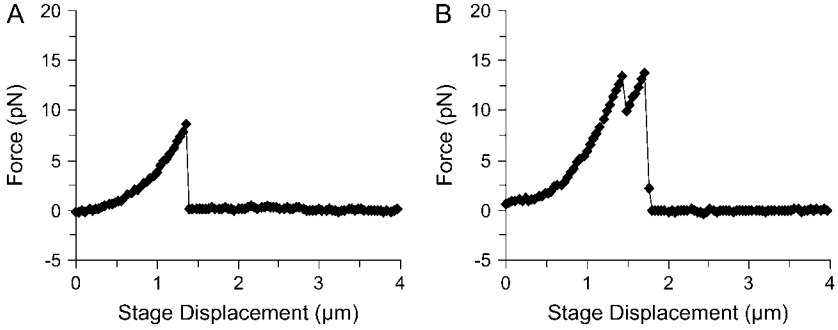

FIGURE 7 Measurement of the strength of poly(U)/ribosome complexes. (*A*) The most common type of behavior, abrupt rupture of the complex. (*B*) Example of a slippage event and then rupture.

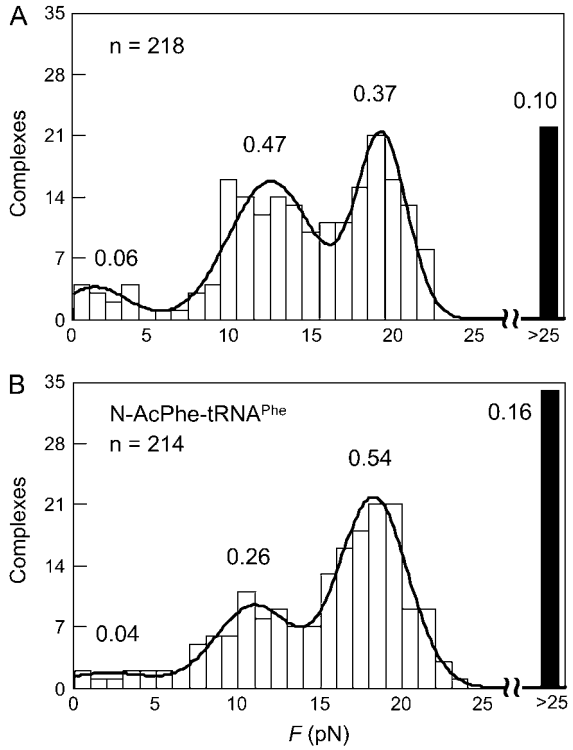

FIGURE 8 Distributions of rupture forces for poly(U)/ribosome complexes in the absence (*A*) and in the presence (*B*) of *N*-AcPhe-tRNA^{Phe}. The number of samples in each histogram is *n*. The curves in *A* and *B* are the results of fitting the sum of three Gaussian components to the data at $F < 25$ pN by maximum likelihood. The black bars represent complexes that did not rupture within the maximum force exerted by the trap (22 complexes in *A* and 34 in *B*). The number next to each peak indicates its fraction of the total.

poly(Phe) synthesis programmed by poly(U) message (31) were retained. However, the birefringence of mica makes it unsuitable for many optical microscopic techniques, and the nonspecific adherence may alter ribosome function.

We developed a new method for specific attachment of ribosomes to glass microscope slides both to have a surface material more suitable for optical studies and to improve the efficiency of ribosome recruitment onto the surface. The results shown in Fig. 2 demonstrate that tethering of streptavidin-coated microspheres to the surface requires all four of the components in the designed linkage: APTES, KMUS cross-linker, ribosomes, and biotinylated poly(U). The *N*-hydroxysuccinimide ester group in KMUS forms a covalent bond with the APTES on the glass surface while the maleimide group at the other end of the KMUS reacts with available Cys residues in the ribosome. When poly(U) was added to the flow chamber in the absence of 70S ribosomes, some tethered beads were observed at a surface density above background, indicating a small amount of poly(U) binding directly to the surface. However, the percentage of bead densities obtained in the absence of 70S ribosomes (fourth pair of *bars* in Fig. 2) to that obtained in the presence of ribosomes (Fig. 2, first pair of *bars*) was markedly higher for the immobilized beads (45%) compared to the tethered beads (4%): i.e., nearly all of the tethered beads were due to ribosome/poly(U) complexes. These results suggest that when poly(U) binds directly to the KMUS surface, it tends to leave only a small segment free at the 3′ end, immobilizing a bead that binds there. A small component of beads bound directly to the surface may also be present. Only when poly(U) is bound to the ribosome does it support formation of tethered complexes, which may indicate that the ribosome functions as a ''platform'' that holds the poly(U) away from the surface.

Slippage and rupture

Since poly(U) does not have a distinct reading frame, it might be expected to slide relatively freely through the mRNA path in the ribosome. The free energy of binding of poly(U) to 70S ribosomes was measured at ~ -56 kJ/mol at room temperature (47), corresponding to ~ 100 pN nm/molecule. It is not straightforward to estimate rupture forces from this thermodynamic quantity, since the amplitude of the rupture force presumably depends on direction and velocity of loading, the distance over which the applicable bonds act, and the buffer conditions, which were different in the above study from those used here. We did observe sudden slippage in the complexes linked to the surface (Fig. 7 *B*) at forces above 10–15 pN. Skinner et al. (48) reported gradual elongation of poly(U) tethers at forces of 8 pN.

A plausible interpretation of the slipping phenomenon is that it corresponds to sliding of poly(U) in the ribosome under the applied force. This explanation implies that 70S ribosomes can bind to a poly(U) molecule at internal locations along its structure. Poly(U) would thus differ from natural mRNA, which is believed to enter the mRNA channel in 70S ribosomes only up to the P-site in the absence of protein synthesis (49). Poly(U) might enter further by threading into the mRNA channel or via direct insertion if the head of the 30S subunit tilts to convert the mRNA channel into a groove (50). Additional support for internal poly(U) binding in 70S complexes comes from the result that the average contour length of the poly(U) molecules (Table 1) is considerably less than the ~ 5 μm value expected if the ribosome could only bind poly(U) at its 5′ end.

Somewhat surprisingly, we find that the rupturing forces partition into several distinct groups (Fig. 8). Such partitioning is unlikely to be due to differences between the direction and onset rate of the applied mechanical force, since the orientation of the ribosomes around the optical axis is random and the rate of force application depends on the tether length (and its resulting compliance). Rather, the components of rupture forces are more probably a consequence of the complexity of interaction between the mRNA and the ribosome, for instance in the A, P, and E sites, or within the decoding center. Further studies of the rupture

force, for example with different mRNAs, tRNAs, and ionic conditions, might permit a more specific explanation.

As 96% of the tethered beads can be attributed to ribosome/poly(U) complexes, it is reasonable to attribute the observed changes in the rupturing forces upon *N*-AcPhe-tRNA^{Phe} addition (Fig. 8, *A* and *B*) to a stabilization of the ribosome-mRNA junction by poly(U)-dependent *N*-AcPhe-tRNA^{Phe} binding to the ribosomal P-site. *N*-AcPhe-tRNA^{Phe} also increased the proportion of ribosome-poly(U)-bead complexes that exhibited slippage before outright rupture, possibly suggesting that added *N*-AcPhe-tRNA^{Phe} increases the likelihood of the ribosome recapturing the poly(U) once it has started slipping. Although the details of the rupture force distributions cannot be unequivocally explained at present, the sizable effects of *N*-AcPhe-tRNA^{Phe} on these distributions, and on the likelihood of slipping and recapture, provide strong support for the conclusion that tethered beads represent authentic ribosome-poly(U)-bead complexes.

Modeling the mechanical properties of poly(U)

E-WLC and E-FJC models both gave reasonably good fits to our F-E data (Fig. 6), as described earlier for ssDNA (51). The best fit (as judged by the value χ_r^2, Fig. 6, Table 1) was obtained with an E-WLC model (16). As expected (18), a simple FJC model does not describe the data well, due to backbone elasticity appreciable at high forces.

As this work was being prepared for publication, analogous measurements of poly(U) elasticity were reported (33). The results, which were determined in the absence of Mg^{2+} and in the presence of either 5 mM or 500 mM NaCl, indicated a strong dependence of the mechanical properties of poly(U) on ionic strength. By comparison, our measurements were performed in the presence of 10 mM Mg^{2+} and an ionic strength of 0.13 M. Despite the different conditions, the value of persistence length, L_p, we obtained using the E-WLC model (0.79 nm, Table 1) is not far from that found by Seol et al. (33) at 500 mM NaCl (0.91 nm) (agreement is less close using the WLC model: 0.57 nm, our data, vs. 0.80 nm). The uncertainty of the estimated L_p in our work, either from the standard error of the mean of the 32 molecules completely analyzed (0.05 nm) or from the average 95% confidence interval in each fit (0.04 nm; range 0.01–0.07 nm), indicates that the value of L_p is well constrained by our data.

The determination of the backbone stiffness, *K*, on the other hand, is subject to larger uncertainties since it mainly depends on the data at the upper limit of forces (80–100 pN) applied here in many, but not all, of the experiments. However, a more robust estimate, based on AFM data on ssDNA collected at higher force, yielded stiffness values of 800–1000 pN (20), very similar to the average we obtained with the E-WLC model (870 pN). This is bracketed by values reported by Seol et al. (33) using lower applied forces (stiffness = 1500–1600 pN at 500 mM Na^+; 450–600 pN at 5 mM Na^+), suggesting that the different ionic strengths and/or specific metal ion:phosphate interactions affect *K*.

L_p values for ssRNA versus ssDNA

In contrast to ssRNA, ssDNA has been studied intensively. Estimates of the persistence length, L_p, of ssDNA appear to be dependent on the experimental approach employed in the measurement. Bulk measurements (light scattering (13); sedimentation (52); diffusion (14); and transient birefringence (12)) have yielded values of 1.5–3 nm. By contrast, single-molecule measurements, conducted using laser tweezers (18), magnetic tweezers (53), and atomic force microscopy (20), and fitted by an E-FJC or E-WLC models, all yielded values of ~0.75 nm. The similarity in the latter value of L_p and the distance between subsequent bases along the backbone of ssDNA (0.7 nm, (44)), is an indication that ssDNA is highly flexible and capable of significant bending on the scale of one or few bases. By comparison, double-stranded DNA has L_p = ~50 nm (16,18).

It has been argued that formation of secondary structure may have increased the apparent L_p in some of the bulk assays on heteropolymeric ssDNA (18) or decreased the apparent L_p in the single-molecule experiments (12,53,54). Our results, showing that L_p for poly(U) is equal to 0.79 nm, essentially identical to the value obtained in single-molecule measurements of ssDNA, provide strong support for the assumption that the elastic properties of RNA are very similar to those of ssDNA (55) and indicate that secondary structure makes little contribution to previously measured L_p values since poly(U) is expected to have no secondary structure. In support of this expectation, we observed no significant hysteresis in our measurements, whereas secondary structures would have produced a different force response during lengthening and shortening (23).

In summary, we have shown that ribosomes attached specifically to the microscope slide surface through a bifunctional cross-linker bind poly(U) and that the mechanical stability of this complex is increased in the presence of *N*-AcPhe-tRNA^{Phe}. F-E curves of poly(U) indicate that the persistence length and backbone rigidity are similar to those of ssDNA. These nucleic acids have virtually complete bending flexibility on the length scale of individual bases.

SUPPLEMENTARY MATERIAL

An online supplement to this article can be found by visiting BJ Online at http://www.biophysj.org.

We thank Dr. M. Ehrenberg, Uppsala University, Sweden for the gift of *N*-acetyl-PhetRNA^{Phe}, Drs. Michael Ostap, Martin Pring, and Serguei Vladimirov for useful discussions, and Ms. Nora Zuno, Mai Pham, and Elizabeth Stone for technical assistance.

The work was supported by National Institutes of Health grant GM63205.

REFERENCES

1. Kennell, D., and H. Riezman. 1977. Transcription and translation initiation frequencies of the *Escherichia coli lac* operon. *J. Mol. Biol.* 114:1–21.
2. Kjeldgaard, N. O., and K. Gausing. 1974. Regulation of biosynthesis of ribosomes. *In* Ribosomes. M. Nomura, A. Tissières, and P. Lengyel, editors. Cold Spring Harbor Laboratory, Cold Spring Harbor, NY. 369–392.
3. Kurland, C. G., and M. Ehrenberg. 1987. Growth-optimizing accuracy of gene expression. *Annu. Rev. Biophys. Biophys. Chem.* 16:291–317.
4. Yusupov, M. M., G. Zh. Yusupova, A. Baucom, K. Lieberman, T. N. Earnest, J. H. D. Cate, and H. F. Noller. 2001. Crystal structure of the ribosome at 5.5 Å resolution. *Science.* 292:883–896.
5. Ramakrishnan, V. 2002. Ribosome structure and the mechanism of translation. *Cell.* 108:557–572.
6. Bashan, A., I. Agmon, R. Zarivach, F. Schluenzen, J. Harms, R. Berisio, H. Bartels, F. Franceschi, T. Auerbach, H. A. S. Hansen, E. Kossoy, M. Kessler, and A. Yonath. 2003. Structural basis of the ribosomal machinery for peptide bond formation, translocation, and nascent chain progression. *Mol. Cell.* 11:91–102.
7. Frank, J. 2003. Electron microscopy of functional ribosome complexes. *Biopolymers.* 68:223–233.
8. Rodnina, M. V., T. Daviter, K. Gromadski, and W. Wintermeyer. 2002. Structural dynamics of ribosomal RNA during decoding on the ribosome. *Biochimie.* 84:745–754.
9. Moore, P. B., and T. A. Steitz. 2003. The structural basis of large ribosomal subunit function. *Annu. Rev. Biochem.* 72:813–850.
10. Rodnina, M. V., and W. Wintermeyer. 2003. Peptide bond formation on the ribosome: structure and mechanism. *Curr. Opin. Struct. Biol.* 13:334–340.
11. Ogle, J. M., and V. Ramakrishnan. 2005. Structural insights into translational fidelity. *Annu. Rev. Biochem.* 74:129–177.
12. Mills, J. B., E. Vacano, and P. J. Hagerman. 1999. Flexibility of single-stranded DNA: use of gapped duplex helices to determine the persistence lengths of poly(dT) and poly(dA). *J. Mol. Biol.* 285:245–257.
13. Achter, E. K., and G. Felsenfield. 1971. The conformation of single-strand polynucleotides in solution: sedimentation studies of apurinic acid. *Biopolymers.* 10:1625–1634.
14. Tinland, B., A. Pluen, J. Sturm, and G. Weill. 1997. Persistence length of single-stranded DNA. *Macromolecules.* 30:5763–5765.
15. Smith, S. B., L. Finzi, and C. Bustamante. 1992. Direct mechanical measurements of the elasticity of single DNA molecules by using magnetic beads. *Science.* 258:1122–1126.
16. Wang, M. D., H. Yin, R. Landick, J. Gelles, and S. M. Block. 1997. Stretching DNA with optical tweezers. *Biophys. J.* 72:1335–1346.
17. Baumann, C. G., V. A. Bloomfield, S. B. Smith, C. Bustamante, M. D. Wang, and S. M. Block. 2000. Stretching of single collapsed DNA molecules. *Biophys. J.* 78:1965–1978.
18. Smith, S. B., Y. Cui, and C. Bustamante. 1996. Overstretching B-DNA: The elastic response of individual double-stranded and single-stranded DNA molecules. *Science.* 271:795–799.
19. Strick, T. R., J.-F. Allemand, D. Bensimon, A. Bensimon, and V. Croquette. 1996. The elasticity of a single supercoiled DNA molecule. *Science.* 271:1835–1837.
20. Rief, M., H. Clausen-Schaumann, and H. E. Gaub. 1999. Sequence-dependent mechanics of single DNA molecules. *Nat. Struct. Biol.* 6:346–349.
21. Bustamante, C., J. F. Marko, E. D. Siggia, and S. Smith. 1994. Entropic elasticity of λ-phage DNA. *Science.* 265:1599–1600.
22. Smith, D. E., S. J. Tans, S. B. Smith, S. Grimes, D. L. Anderson, and C. Bustamante. 2001. The bacteriophage ϕ29 portal motor can package DNA against a large internal force. *Nature.* 413:748–752.
23. Liphardt, J., B. Onoa, S. B. Smith, I. Tinoco Jr., and C. Bustamante. 2001. Reversible unfolding of single RNA molecules by mechanical force. *Science.* 292:733–737.
24. Wang, M. D., M. J. Schnitzer, H. Yin, R. Landick, J. Gelles, and S. M. Block. 1998. Force and velocity measured for single molecules of RNA polymerase. *Science.* 282:902–907.
25. de Smit, M. H., and J. van Duin. 1990. Secondary structure of the ribosome binding site determines translational efficiency: a quantitative analysis. *Proc. Natl. Acad. Sci. USA.* 87:7668–7672.
26. Voges, D., M. Watzele, C. Nemetz, S. Wizemann, and B. Buchberger. 2004. Analyzing and enhancing mRNA translational efficiency in an *Escherichia coli* in vitro expression system. *Biochem. Biophys. Res. Commun.* 318:601–614.
27. Plant, E. P., K. L. M. Jacobs, J. W. Harger, A. Meskauskas, J. L. Jacobs, J. L. Baxter, A. N. Petrov, and J. D. Dinman. 2003. The 9-Å solution: how mRNA pseudoknots promote efficient programmed -1 ribosomal frameshifting. *RNA.* 9:168–174.
28. Blanchard, S. C., H. D. Kim, R. L. Gonzalez Jr., J. D. Puglisi, and S. Chu. 2004. tRNA dynamics on the ribosome during translation. *Proc. Natl. Acad. Sci. USA.* 101:12893–12898.
29. Blanchard, S. C., R. L. Gonzalez Jr., H. D. Kim, S. Chu, and J. D. Puglisi. 2004. tRNA selection and kinetic proofreading in translation. *Nat. Struct. Mol. Biol.* 11:1008–1014.
30. Sytnik, A., S. Vladimirov, Y. Jia, L. Li, B. S. Cooperman, and R. M. Hochstrasser. 1999. Peptidyl transferase center activity observed in single ribosomes. *J. Mol. Biol.* 285:49–54.
31. Vanzi, F., S. Vladimirov, C. R. Knudsen, Y. E. Goldman, and B. S. Cooperman. 2003. Protein synthesis by single ribosomes. *RNA.* 9: 1174–1179.
32. Vanzi, F., Y. Takagi, S. Vladimirov, H. Shuman, B. S. Cooperman, and Y. E. Goldman. 2003. Single-molecule mechanics of poly(U): elastic properties and interactions with ribosomes. *Biophys. J.* 84:299a. (Abstr.)
33. Seol, Y., G. M. Skinner, and K. Visscher. 2004. Elastic properties of a single-stranded charged homopolymeric ribonucleotide. *Phys. Rev. Lett.* 93:118102–1-118102–4.
34. Vanzi, F., S. Vladimirov, C. R. Knudsen, B. S. Cooperman, and Y. E. Goldman. 2001. Peptide synthesis by single ribosomes. *Biophys. J.* 80:157a. (Abstr.)
35. Litvinov, R. I., H. Shuman, J. S. Bennett, and J. W. Weisel. 2002. Binding strength and activation state of single fibrinogen-integrin pairs on living cells. *Proc. Natl. Acad. Sci. USA.* 99:7426–7431.
36. Visscher, K., S. P. Gross, and S. M. Block. 1996. Construction of multiple-beam optical traps with nanometer-resolution position sensing. *IEEE J. Selec. Top. in Quant. Electr.* 2:1066–1076.
37. Allersma, M. W., F. Gittes, M. J. deCastro, R. J. Stewart, and C. F. Schmidt. 1998. Two-dimensional tracking of ncd motility by back focal plane interferometry. *Biophys. J.* 74:1074–1085.
38. Nakajima, H., and H. Ogawa. 1992. Compact Disc Technology. Ohmsha Ltd., Tokyo.
39. Happel, J., and H. Brenner. 1981. Low Reynolds Number Hydrodynamics with Special Applications to Particulate Media. Sijthoff & Noordhoff, Dordecht, The Netherlands.
40. Svoboda, K., and S. M. Block. 1994. Biological applications of optical forces. *Annu. Rev. Biophys. Biomol. Struct.* 23:247–285.
41. Muralikrishna, P., and B. S. Cooperman. 1991. A photolabile oligodeoxyribonucleotide probe of the peptidyltransferase center: identification of neighboring ribosomal components. *Biochemistry.* 30:5421–5428.
42. Rappoport, S., and Y. Lapidot. 1974. The chemical preparation of acetylaminoacyl-tRNA. *Methods Enzymol.* 29:685–688.
43. Press, W. H., S. A. Teukolsky, W. T. Vetterling, and B. P. Flannery. 1992. Numerical Recipes in C: The Art of Scientific Computing. Cambridge University Press, New York.
44. Saenger, W. 1984. Principles of Nucleic Acid Structure. Springer-Verlag, New York.

45. Fisher, R. A. 1958. Statistical Methods for Research Workers, 13th ed. Tweeddale Court, London.

46. Karlsson, M., M. Yu. Pavlov, M. Malmqvist, B. Persson, and M. Ehrenberg. 1999. Initiation of *Escherichia coli* ribosomes on matrix coupled mRNAs studied by optical biosensor technique. *Biochimie*. 81:995–1002.

47. Katunin, V. I., Yu. P. Semenkov, V. I. Makhno, and S. V. Kirillov. 1980. Comparative study of the interaction of polyuridylic acid with 30S subunits and 70S ribosomes of Escherichia coli. *Nucleic Acids Res.* 8:403–421.

48. Skinner, G. M., Y. Seol, K. H. Nierhaus, and K. Visscher. 2004. Translocation and force-induced slippage of individual ribosomes along messenger RNA. *Biophys. J.* 86:316a. (Abstr.)

49. Moll, I., S. Grill, C. O. Gualerzi, and U. Bläsi. 2002. Leaderless mRNAs in bacteria: surprises in ribosomal recruitment and translational control. *Mol. Microbiol.* 43:239–246.

50. Ogle, J. M., F. V. Murphy IV, M. J. Tarry, and V. Ramakrishnan. 2002. Selection of tRNA by the ribosome requires a transition from an open to a closed form. *Cell.* 111:721–732.

51. Bustamante, C., S. B. Smith, J. Liphardt, and D. Smith. 2000. Single-molecule studies of DNA mechanics. *Curr. Opin. Struct. Biol.* 10: 279–285.

52. Inners, L. D., and G. Felsenfeld. 1970. Conformation of polyribouridylic acid in solution. *J. Mol. Biol.* 50:373–389.

53. Maier, B., D. Bensimon, and V. Croquette. 2000. Replication by a single DNA polymerase of a stretched single-stranded DNA. *Proc. Natl. Acad. Sci. USA.* 97:12002–12007.

54. Rouzina, I., and V. A. Bloomfield. 2001. Force-induced melting of the DNA double helix 1. Thermodynamic analysis. *Biophys. J.* 80:882–893.

55. Gerland, U., R. Bundschuh, and T. Hwa. 2001. Force-induced denaturation of RNA. *Biophys. J.* 81:1324–1332.